Mutations in *FYCO1* Cause Autosomal-Recessive Congenital Cataracts

Jianjun Chen,[1,9] Zhiwei Ma,[1,9] Xiaodong Jiao,[1] Robert Fariss,[2] Wanda Lee Kantorow,[3] Marc Kantorow,[3] Eran Pras,[4] Moshe Frydman,[5] Elon Pras,[5] Sheikh Riazuddin,[6,7] S. Amer Riazuddin,[6,8,10] and J. Fielding Hejtmancik[1,10,*]

Congenital cataracts (CCs), responsible for about one-third of blindness in infants, are a major cause of vision loss in children worldwide. Autosomal-recessive congenital cataracts (arCC) form a clinically diverse and genetically heterogeneous group of disorders of the crystalline lens. To identify the genetic cause of arCC in consanguineous Pakistani families, we performed genome-wide linkage analysis and fine mapping and identified linkage to 3p21-p22 with a summed LOD score of 33.42. Mutations in the gene encoding FYVE and coiled-coil domain containing 1 (*FYCO1*), a PI(3)P-binding protein family member that is associated with the exterior of autophagosomes and mediates microtubule plus-end-directed vesicle transport, were identified in 12 Pakistani families and one Arab Israeli family in which arCC had previously been mapped to the overlapping CATC2 region. Nine different mutations were identified, including c.3755 delC (p.Ala1252AspfsX71), c.3858_3862dupGGAAT (p.Leu1288TrpfsX37), c.1045 C>T (p.Gln349X), c.2206C>T (p.Gln736X), c.2761C>T (p.Arg921X), c.2830C>T (p.Arg944X), c.3150+1 G>T, c.4127T>C (p.Leu1376Pro), and c.1546C>T (p.Gln516X). *Fyco1* is expressed in the mouse embryonic and adult lens and peaks at P12d. Expressed mutant proteins p.Leu1288TrpfsX37 and p.Gln736X are truncated on immunoblots. Wild-type and p.L1376P FYCO1, the only missense mutant identified, migrate at the expected molecular mass. Both wild-type and p. Leu1376Pro FYCO1 proteins expressed in human lens epithelial cells partially colocalize to microtubules and are found adjacent to Golgi, but they primarily colocalize to autophagosomes. Thus, *FYCO1* is involved in lens development and transparency in humans, and mutations in this gene are one of the most common causes of arCC in the Pakistani population.

A significant cause of vision loss worldwide, congenital cataracts (CC) cause approximately one-third of the cases of blindness in infants.[1] They can occur in an isolated fashion or as one component of a syndrome affecting multiple tissues, although the distinction might be somewhat arbitrary in some cases. In approximately 70% of CC cases, the lens alone is involved.[2] Nonsyndromic CCs have an estimated frequency of 1–6 per 10,000 live births,[3] and approximately one-third of CC cases are familial.[4] Congenital cataracts are very heterogeneous, both clinically and genetically, and approximately 8.3%–25% of nonsyndromic CCs are inherited as an autosomal-recessive (ar), autosomal-dominant (ad), or X-linked trait.[5–7] To date, more than 40 loci for human CCs have been identified, and more than 26 of them have been associated with causative mutations in specific genes.[8] To date, 14 genetic loci have been implicated in nonsyndromic autosomal-recessive CC (arCC), and most of these account for a few percentage points of CC cases each. Among these loci, mutations in nine genes, eph-receptor type-A2 (*EPHA2,* MIM 613020), connexin50 (*GJA8,* MIM 600897), glucosaminyl (N-acetyl) transferase 2 (*GCNT2,* MIM 600429), heat-shock transcription factor 4 (*HSF4*, MIM 602438), lens intrinsic membrane protein (*LIM2*, MIM 154045), beaded filament structural protein 1 (*BFSP1*, MIM 603307), αA-crystallin (*CRYAA*, MIM 123580), βB1-crystallin (*CRYBB1*, MIM 600929), and βB3-crystallin (*CRYBB3*, MIM 123630), have been found.[9–18] In six of the 14 reported arCC loci, the mutated gene is as yet unknown. The CATC2 (Cataract, Autosomal Recessive Congenital 2, MIM 610019) locus was first mapped to chromosome 3 in three inbred Arab families in 2001, but the disease-associated variants previously had not been identified.[19]

As part of an ongoing collaboration between the National Eye Institute (NEI, Bethesda, MD, USA), the National Centre of Excellence in Molecular Biology (NCEMB, Lahore, Pakistan), and Allama Iqbal Medical College (Lahore, Pakistan), a locus for arCC in twelve Pakistani families has been mapped to chromosomal region 3p21-p22, overlapping the CATC2 locus.[19] Subsequently, homozygous missense, splice site, nonsense, and frameshift mutations have been identified in a positional candidate gene, *FYCO1* (FYVE and coiled-coil domain containing 1 [MIM 607182]). In addition, a nonsense mutation was found in an Arab Israeli family in which the CATC2 locus had been

[1]Ophthalmic Genetics and Visual Function Branch, National Eye Institute, National Institutes of Health, Bethesda, MD 20892, USA; [2]Imaging Core, National Eye Institute, National Institutes of Health, Bethesda, MD 20892, USA; [3]Department of Biomedical Science, Florida Atlantic University, room 207, Biomedical building, 777 Glades Rd. Boca Raton, FL, USA; [4]Department of Ophthalmology, Assaf Harofeh Medical Center, Zerifin, Israel; affiliated with the Sackler School of Medicine, Tel Aviv University, Tel Aviv, Israel; [5]The Danek Gertner Institute of Human Genetics, Sheba Medical Center, Ramat Gan, Israel; affiliated with the Sackler School of Medicine, Tel Aviv University, Tel Aviv, Israel; [6]National Centre of Excellence in Molecular Biology, University of the Punjab, Lahore 53700, Pakistan; [7]Allama Iqbal Medical College, Lahore 54550, Pakistan; [8]The Wilmer Eye Institute, Johns Hopkins University School of Medicine, Baltimore, MD 21287, USA
[9]These authors contributed equally to this work
[10]These authors contributed equally to this work
*Correspondence: f3h@helix.nih.gov
DOI 10.1016/j.ajhg.2011.05.008.

mapped. In total, 9 *FYCO1* mutations were identified in 13 arCC families, including 44 affected individuals, in which arCC segregates with the mutant *FYCO1* allele, underlining the importance of *FYCO1* in both lens biology and the pathogenesis of arCC.

In this study, genome-wide linkage scans and fine mapping were performed in eight unrelated consanguineous arCC families of Pakistani origin, and 63 additional unlinked consanguineous families of Pakistani origin were additionally screened for mutations in *FYCO1*. Families described in this study include 060003 (also referred to as PKCC003), 060012 (PKCC012), 060014 (PKCC014), 060031 (PKCC031), 060041 (PKCC041), 060044 (PKCC044), 060054 (PKCC054), 060058 (PKCC058), 060064 (PKCC064), 060069 (PKCC069), 060091 (PKCC091), and 060094 (PKCC094). This study was approved by Institutional Review Board (IRB) of the National Centre of Excellence in Molecular Biology and the CNS IRB at the National Institutes of Health. Participating subjects gave informed consent consistent with the tenets of the Declaration of Helsinki. Ophthalmological examinations were performed at the Layton Rahmatullah Benevolent Trust Hospital, Lahore, Pakistan. A detailed medical history was obtained by interviewing family members. Medical records of clinical exams conducted with slit lamp biomicroscopy reported the types of cataract in affected individuals of the twelve families. We also recruited 150 unrelated, ethnically matched individuals, who provided control DNA samples. Blood samples were obtained from study participants and DNA was extracted using standard inorganic methods as previously described.[20] All affected individuals available for examination from twelve consanguineous Pakistani arCC families (060003, 060012, 060014, 060031, 060041, 060044, 060054, 060058, 060064, 060069, 060091, and 060094) displayed bilateral nuclear cataracts that either were present at birth or developed in infancy (Figure 1). Some affected individuals had undergone cataract surgery in the early years of life, and hence no pictures of their lenses were available. Autosomal recessive inheritance of the cataracts was seen in all families (Figure 2A). No other ocular or systemic abnormalities were present in these families.

Genome-wide linkage analysis was completed with 382 highly polymorphic microsatellite markers from the ABI PRISM Linkage Mapping Set MD-10 (Figure S2, available online; average spacing 10 cM; Applied Biosystems, Foster City, CA). PCR products were separated on an ABI 3130 DNA Analyzer, and alleles were assigned with GeneMapper Software version 4.0 (Applied Biosystems). Two-point linkage analyses were performed with the FASTLINK version of MLINK from the LINKAGE Program Package.[21,22] Maximum LOD scores were calculated with ILINK. Autosomal-recessive cataracts were analyzed as a fully penetrant trait with a disease allele frequency of 0.001, and equal allele frequencies were arbitrarily used for all markers in the genome-wide scan. Marker allele frequencies were calculated from 100 Pakistani control individuals for fine mapping (Table S3). The marker order and distances between the markers were obtained from the Marshfield database and the NCBI chromosome 3 sequence maps (see Table S1). Eight of these families (060003, 060012, 060041, 060058, 060064, 060069, 060091, and 060094) independently showed significant or suggestive linkage to chromosomal region 3p21-p22; LOD scores were 3.85, 2.52, 4.09, 2.36, 3.89, 5.62, 4.88, and 3.82, respectively.

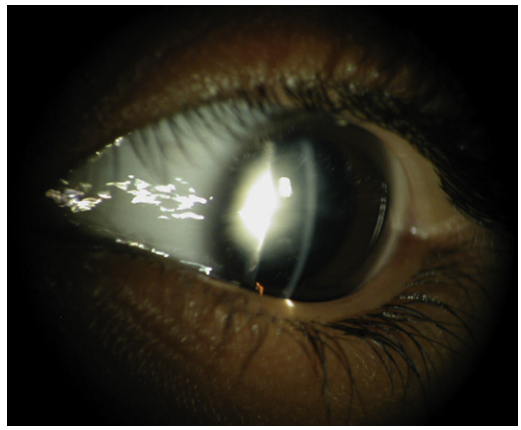

Figure 1. Slit-Lamp Photograph of a Cataract Patient with *FYCO1* Mutations
A slit-lamp photograph of affected individual 19 of family 060069 shows a nuclear cataract that developed in early infancy.

Sequencing of candidate genes (see below) identified *FYCO1* mutations in affected members of these eight families and subsequently in four additional arCC families (see below). Two-point linkage analysis in the 12 families with *FYCO1* mutations confirms linkage to a 7.4 cM (15.6 Mb) region flanked by D3S3521 and D3S1289 (Table 1). The linked region includes markers D3S3582 ($Z_{max} = 33.4$ at $\theta = 0$), D3S3561 ($Z_{max} = 22.4$ at $\theta = 0$), D3S3685 ($Z_{max} = 33.5$ at $\theta = 0.01$), and D3S2407 ($Z_{max} = 24$ at $\theta = 0.03$). Significant LOD scores were also seen with other markers in the region, including *D3S3512* ($Z_{max} = 16.75$ at $\theta = 0.08$), *D3S3521* ($Z_{max} = 18.15$ at $\theta = 0.05$), *D3S1289* ($Z_{max} = 25.86$ at $\theta = 0.02$), *D3S3616* ($Z_{max} = 20.14$ at $\theta = 0.05$), *D3S1300* ($Z_{max} = 14.29$ at $\theta = 0.09$), and *D3S3698* ($Z_{max} = 2.14$ at $\theta = 0.2$), although these markers show obligate recombination events. Haplotype analysis confirmed and narrowed the critical interval (Figure 2B and Figure S1). Key recombination events were detected between markers D3S3582 and the adjacent telomeric marker D3S3685 in affected individuals 22, 26, 28, and 30 of family 060091 (Figure 2B and Figure S1), so that D3S3685 defines the telomeric boundary for the 3.5 cM (12 Mb) disease interval. Similarly, recombination events were detected between marker D3S3561 and its adjacent centromeric marker D3S1289 in individual 14 of family 060041, individuals 3, 7, and 8 of family 060064, and individual 26 of 060094 (Figure 2B and Figure S1), so that D3S1289 is the centromeric flanking marker. Thus, arCC in each of these 12 families cosegregates with a chromosome 3 region that includes *FYCO1*.

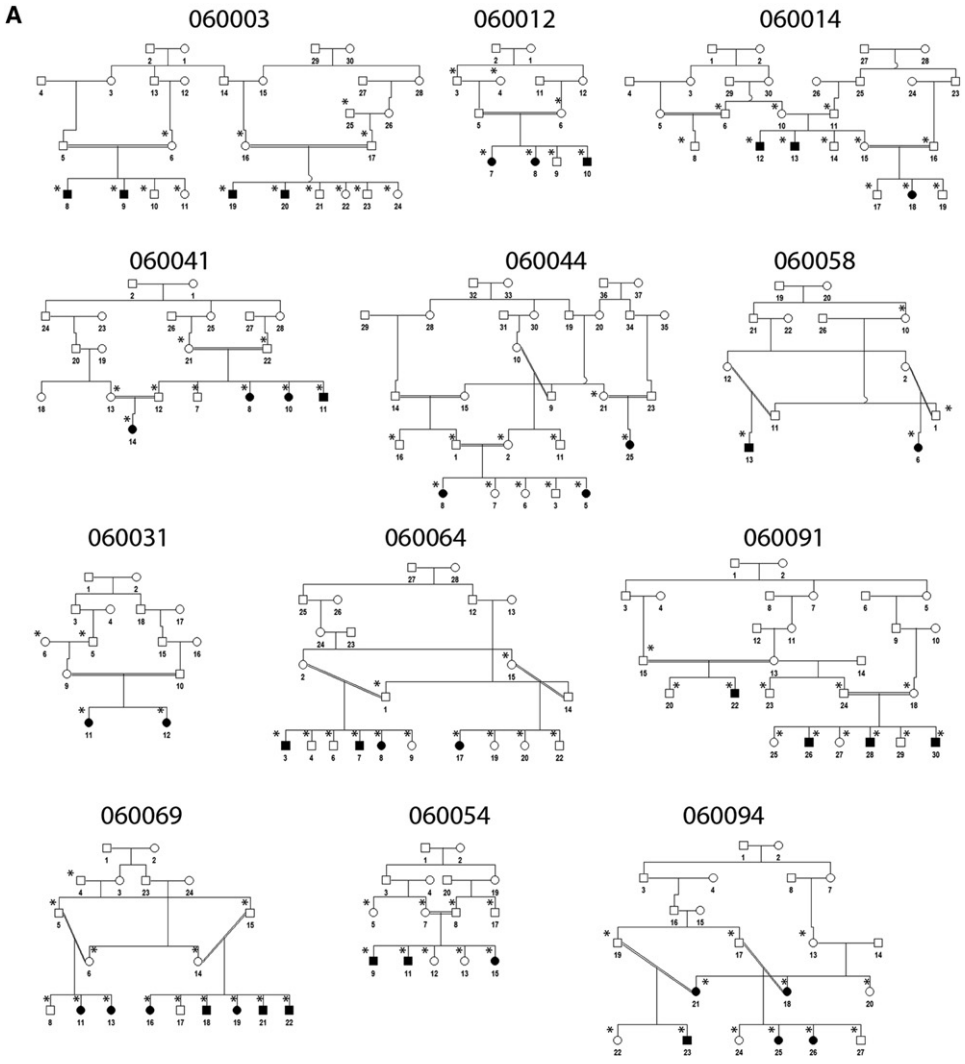

Figure 2. Pedigrees and Linkage Intervals for arCC Families

(A) Twelve arCC pedigrees collected from Pakistan. Filled symbols denote affected individuals. Eight pedigrees (060003, 060012, 060041, 060058, 060064, 060069, 060091, and 060094) were used for genome-wide linkage scans and fine mapping of arCC intervals and candidate-gene mutation screenings. Four pedigrees (060014, 060031, 060044, and 060054) were used for fine mapping of arCC intervals and candidate-gene mutation screenings. Individuals who were genotyped are marked with an asterisk.

(B) Refined arCC interval on the basis of haplotype analysis of patients with recombination events. Markers with the homozygous genotype are boxed so that the region without recombination is defined. Alleles for markers *D3S3685* and *D3S1289* in patients with recombination events are in bold so that the telomeric and centromeric breakpoints, respectively, are shown. The disease interval was placed between markers *D3S3685* and *D3S1289*.

Table 1. Two-Point LOD Scores of Markers on Chromosomal Region 3p21 in a Total of 12 arCC Families

Marker	cM	Mb	0	0.01	0.05	0.1	0.2	0.3	0.4	Zmax	θmax
D3S3512	61.52	34.59	- ∞	12.29	16.28	16.64	13.85	9.42	4.56	16.75	0.08
D3S3521	63.12	38.87	- ∞	15.69	18.15	17.21	13.1	8.2	3.5	18.15	0.05
D3S2407	67.94	41.39	16.94	23.58	23.63	21.72	16.55	10.74	4.98	24.02	0.03
D3S3685	67.94	42.47	32.7	33.5	31.4	28.09	20.87	13.32	6.07	33.5	0.01
D3S3582	69.19	45.39	33.42	32.77	30.14	26.74	19.63	12.36	5.54	33.42	0
D3S3561	70.61	52.34	22.37	21.88	19.9	17.4	12.35	7.43	3.09	22.37	0
D3S1289*	71.41	54.48	- ∞	25.62	25.05	22.56	16.45	9.93	3.99	25.86	0.02
D3S3616	76.48	57.34	- ∞	17.11	20.14	19.28	14.79	9.15	3.94	20.14	0.05
D3S1300*	80.32	60.51	- ∞	7.01	13.46	14.25	11. 8	7.75	3.54	14.29	0.09
D3S3698	84.92	63.12	- ∞	−17.66	−4.57	−0.21	2.14	1.93	0.99	2.14	0.2

An asterisk indicates that an STR marker was included in the genome-wide scan.

The linked region on chromosome 3 contains 287 genes or potential genes, according to the UCSC database. Candidate genes were prioritized on the basis of their expression in the lens and possible function in lens biology and transparency, as indicated in the NCBI and GeneCard databases. Although no candidate genes were absolutely excluded, pseudogenes, genes of unknown function and without known domain structures, and genes not expressed in the lens were given the lowest priorities. Primer pairs for individual exons in the critical interval were designed with the online primer3 program. The sequences and amplification conditions for *FYCO1* primers are available in Table S2. The PCR primers for each exon were used for bidirectional sequencing with Big Dye Terminator Ready reaction mix according to instructions of the manufacturer (Applied Biosystems, Foster City, CA). Sequencing was performed on an ABI PRISM 3130 automated sequencer (Applied Biosystems, Foster City, CA). Sequence traces were analyzed with Mutation Surveyor (Soft Genetics Inc., State College PA) and the Seqman program of DNASTAR Software (DNASTAR Inc, Madison, WI, USA).

After family 060064 was screened for 35 genes in the linked region (all of these genes were found to lack pathogenic mutations), the FYVE and coiled-coil domain containing 1 (*FYCO1*) gene was sequenced, and mutations were identified in this family and subsequently in the remaining seven linked families (NM_024513.2, Table 2 and Figure 3). Mutations were confirmed in all available affected family members. In family 060064, the affected individuals carry a homozygous C>T transition (1045 C>T) in exon 8, which

Table 2. *FYCO1* Mutations in 13 arCC Families

Family	Allele Sharing	Maximum LOD Score	Exon	Nucleotide Change	Predicted Amino Acid Change
060064	no	3.89	8	c.1045 C>T	p.Gln349X
060003	yes	3.85	8	c.2206C>T	p.Gln736X
060012	yes	2.52	8	c.2206C>T	p.Gln736X
060069	yes	5.62	8	c.2206C>T	p.Gln736X
060054	no	2.61	8	c.2761C>T[a]	p.Arg921X
060041	no	4.09	8	c.2830C>T[a]	p.Arg944X
060044	no	2.53	9	c.3150+1 G>T	inactivation of splice donor site
060091	no	4.88	13	c.3755 delC	p.Ala1252AspfsX71
060094	yes	3.82	14	c.3858_3862dupGGAAT	p.Leu1288TrpfsX37
060014	yes	2.73	14	c.3858_3862dupGGAAT	p.Leu1288TrpfsX37
060058	yes	2.36	16	c.4127T>C	p.Leu1376Pro
060031	yes	2.28	16	c.4127T>C	p.Leu1376Pro
Family 1[19]	no	n/a	8	c.1546C>T	p.Gln516X

Nucleotide and amino acid designations are based on Refseq NM_024513.2.
[a] These C>T changes occurred in a CpG dinucleotide.

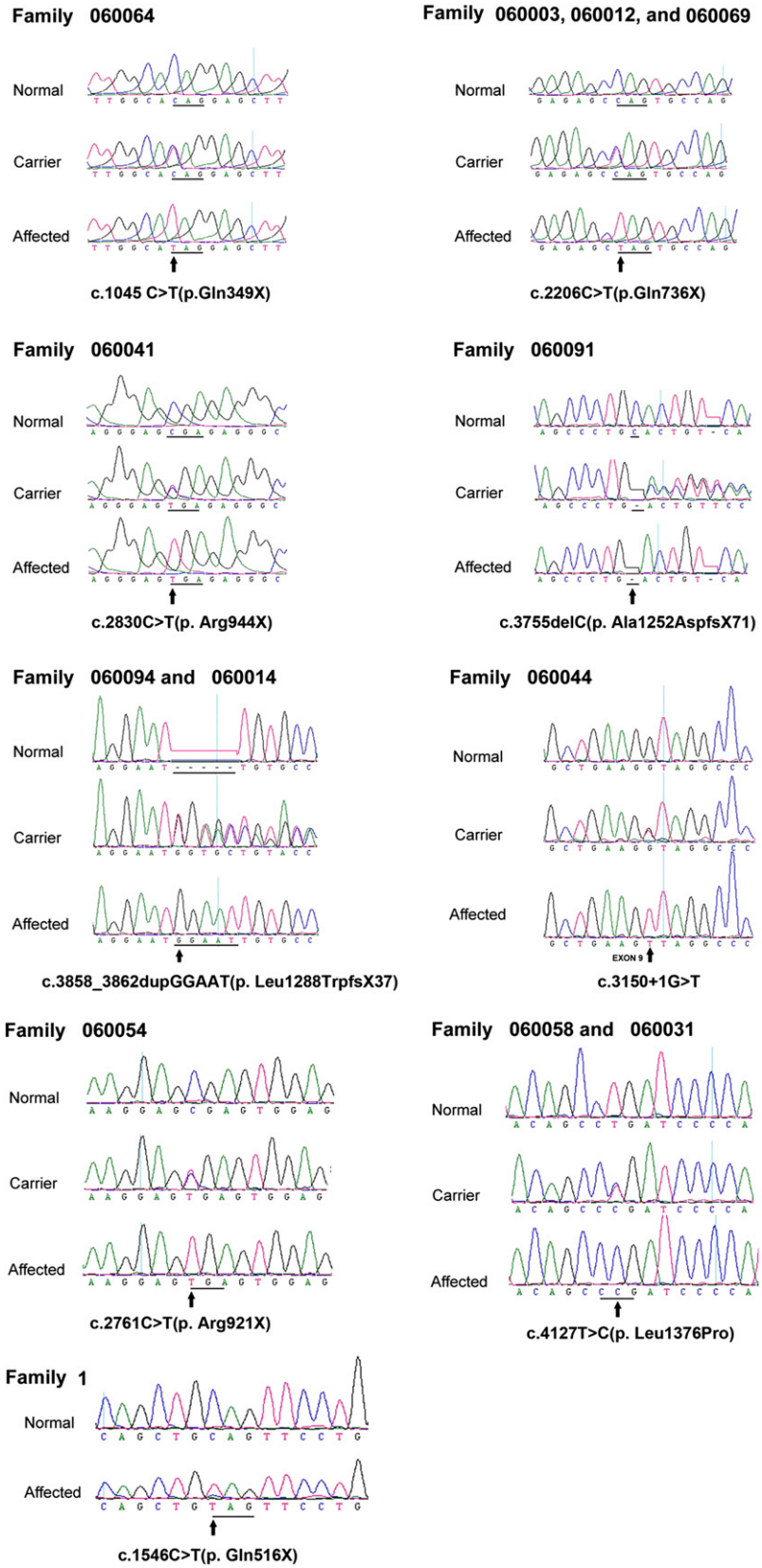

Figure 3. Sequence Electropherograms of the Eight Homozygous Mutations Found in *FYCO1* and Associated with arCC

Wild-type sequence from normal control individuals is shown in the top panel for comparison. The c.1045C>T (p.Gln349X), c.1546C>T (p.Gln516X)), c.2206C>T (p.Gln736X), c.2761C>T (p. Arg921X), and c.2830C>T (p. Arg944X) mutations result in the generation of a stop codon; the c.3755 delC (Ala1252AspfsX71) and c.3858_3862dupGGAAT (p.Leu1288TrpfsX37) mutations lead to a frameshift and a premature termination of translation; the c. 3150+1 G>T mutation leads to elimination of the intron 9 donor site; and the c.4127T>C (p.Leu1376Pro) mutation results in the change of a leucine residue to a proline residue in exon 16.

results in a premature termination of translation (p.Gln349X). Three families (060003, 060012, and 060069) share a homozygous C>T transition (2206 C>T) in exon 8, and this transition results in a putative premature termination of translation or nonsense-mediated decay (p.Gln736X). These families share a common haplotype of 14 consecutive SNP markers across *FYCO1,* suggesting that they derive the mutant allele from a common ancestor (Table 3). In family 060041, a homozygous single base change in exon 8 converts an arginine residue to a premature stop codon (c.2830C>T; p.Arg944X). In family 060091, a homozygous single base-pair deletion in exon 13 causes a frameshift (c.3755 delC, p.Ala1252AspfsX71) resulting in a putative stop codon 71 amino acids downstream. In family 060094, affected individuals carry a homozygous 5 bp exon 14 duplication causing a frameshift (c.3858_3862dupGGAAT, p.Leu1288TrpfsX37) and putative stop codon 37 amino acids downstream. In family 060058, affected individuals carry a homozygous single base change converting a leucine to a proline residue in exon 16 (c.4127T>C; p.Leu1376Pro).

Linkage analysis in some of the 125 arCC families ascertained had mapped loci to regions other than 3p21-p22. Sequencing FYCO1 in an affected individual from each of the 63 families in whom linkage analysis had not yielded a maximal LOD score of 3 identified mutations in four additional families (Table 2 and Figure 3). In family 060054, a homozygous single base change in exon 8 converts an arginine residue to a premature stop codon (c.2761C>T; p.Arg921X). In family 060044, we identified a homozygous single base change, a G-to-T transversion located in the conserved intron 9 donor splice site (c. 3150+1 G>T), suggesting that it might affect splicing.

Table 3. Intragenic FYCO1 Haplotypes of Families Sharing Common Mutations

				p.Gln736X			p.Leu1288TrpfsX37		p.Leu1376Pro	
PCR Amplicon	Position	SNP ID	Allele (Frequency)	Family 060003	Family 060012	Family 060069	Family 060094	Family 060014	Family 060031	Family 060058
4	45961218	rs4682801	C(.07)/A(.93)	A	A	A	A	A	A	A
5	45956851	rs751552	T(.71)/A(.29)	T	T	T	A	A	T	T
6	45954545	rs41289622	A(.61)/C(.39)	C	C	C	A	A	A	A
8A	45950077	rs4683158	G(.07)/A(.93)	A	A	A	A	A	A	A
8A	45950007	rs13071283	A(.61)/G(.39)	G	G	G	A	A	A	A
8B	45949864	rs3733100	G(.56)/C(.44)	C	C	C	C	C	G	G
8C	45949487	rs33910087	C(.67)/T(.33)	T	T	T	C	C	C	C
8E	45948790	rs3796375	C((.73)/T(.27)	C	C	C	T	T	C	C
8G	45948087	rs13079869	C(.7)/T(.3)	T	T	T	C	C	C	C
8H	45947825	rs71622515	AAC(.61)/GAA(.39)	GAA	GAA	GAA	AAC	AAC	AAC	AAC
8H	45947702	rs1994490	A(.39)/G(.61)	G	G	G	G	G	A	A
12	45940870	rs13069079	C(.61)/T(.39)	T	T	T	C	C	C	C
14	45936761	rs1463680	C(.18)/T(.82)	T	T	T	T	T	T	T
15	45917899	rs1873002	A(.16)/G(.84)	G	G	G	G	G	G	G
Fi[a]				.00019	.00019	.00019	.000813	.000813	.00162	.00162
FH_{CHM}[b]				0.019	0.019	0.019	0.026	0.026	0.037	0.037

The PCR amplicon, as well as the SNP, its position in the Ref_Assembly Build 37.1, SNP ID, and allelic variants are shown. Haplotypes were constructed on the basis of 14 consecutive intragenic single nucleotide polymorphisms (SNPs) within *FYCO1*.
[a] Fi: Frequency of the haplotype calculated on an assumption of independent inheritance of all SNP alleles estimated from 48 unrelated Pakistani controls.
[b] FH_{CHM}: Frequency of the haplotype calculated from 48 unrelated Pakistani controls via the CHM algorithm as implemented in the Golden Helix SVS package.

This is supported by the calculated splice-site scores of 7.6 for the normal splice site and −3.2 for the variant site, predicting that the c. 3150+1 G>T change leads to elimination of the intron 9 donor site. As in family 060094, exon 14 of affected individuals in family 060014 contains a homozygous 5 bp duplication causing a frameshift. The families share a common 14 intragenic *FYCO1* SNP haplotype, suggesting that the mutant allele originates from a common ancestor (Table 3). As in family 060058, exon 16 of affected individuals in family 060031 contains a homozygous single base change that converts a leucine residue to a proline residue (c.4127T>C; p.Leu1376Pro). Once more, these two families share a common 14 SNP intragenic *FYCO1* haplotype, suggesting that the disease allele originates from a common ancestor (Table 3). Each of the identified mutations segregates with arCC in the families, and none is present in the NCBI or Ensemble SNP databases. In addition, none of these eight mutations was detected in 300 unrelated, ethnically matched control chromosomes or in HapMap samples of any ethnicity. In addition, *FYCO1* was sequenced in family 1 from Pras et al.,[19] and the finding of a homozygous c.1546C>T sequence change (p.Gln516X) indicates that the *FYCO1* mutation causes the autosomal-recessive congenital cataracts in this consanguineous Arabic family (Figure 3) and thus is the gene mutated in CATC2.

FYCO1 on chromosome 3 contains 18 exons comprising 79 Kb and encoding 1478 amino acids.[23,24] The full-length FYCO1 mRNA (NM_024513.2) encodes a 167 kDa protein. FYCO1 has been highly conserved throughout evolution (protein sequence identity between humans and dogs after alignment via the CLUSTALW algorithm is 81%; that between humans and cows is 81%, that between humans and mice is 78%, that between humans and platypuses is 66%, and that between humans and zebrafish is 37%). Analyses using the Conserved Domain Database[25] and the COILS web server[26] predict that FYCO1 is a long coiled-coil protein similar to members of two families of Rab effector proteins: RUN and FYVE domain-containing proteins (RUFY1–4) and early endosome antigen 1 (EEA1).[27] FYCO1 contains a long central coiled-coil region flanked at the N terminus by an α-helical RUN domain or a zinc finger domain and at the C terminus by a FYVE domain (Figure 4A). Unique to FYCO1 is the presence of a C-terminal extension in the form of a GOLD (Golgi dynamics) domain and an unstructured loop region connecting the FYVE and GOLD domains (Figure 4A). Most of the identified mutations truncate the protein and are predicted to cause termination of the peptide chain before the GOLD domain structure is formed and so to result in loss of activity. In addition, these truncation mutations occur in internal exons,

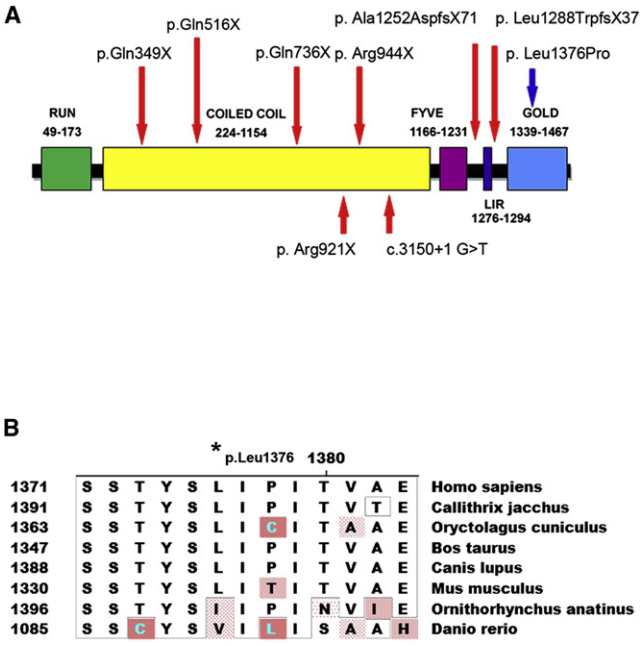

Figure 4. FYCO1 Domain Structure and Mutations
(A) Schematic diagram of FYCO1, showing the locations and effects of the recessive mutations. Domain structure of FYCO1. FYVE represents the FYVE zinc-finger domain; LIR represents the LC3-interacting region; and GOLD represents the Golgi dynamics domain. Red arrows show the positions of the truncation mutations associated with arCC, and the blue arrow shows the missense mutation p.Leu1376Pro.
(B) Amino acid sequence alignment around the FYCO1 Leu1376 amino acid (asterisk) in eight species, ranging from humans to zebrafish.

making these mRNAs potential targets for nonsense-mediated decay.

A single missense mutation, Leu1376Pro, was observed in two families, 060031 and 060058. Occurrence in two unrelated families, segregation with the disease in these two families, and absence in ethnically matched control samples strongly suggests that p.Leu1376Pro might be causative rather than a benign variant. The p.Leu1376Pro missense mutation disrupts a residue conserved from humans to mouse (L1376) within the GOLD domain, suggesting that it is critical for protein function (Figure 4B). In addition, L1376 is conserved in various mammalian species as divergent as cows, dogs, mice, rabbits, and marmosets and shows only conservative changes to isoleucine and valine in platypuses and zebrafish, respectively (Figure 4B). The p.Leu1376Pro change was scored (1.79) as "possibly damaging" for protein function with PolyPhen and as "not tolerated" by SIFT algorithms. Also, the Blosum80 matrix score for this amino acid change indicates that it is potentially damaging for protein function. However, final confirmation of the causative role of this mutation awaits functional assays.

FYCO1 is reported to be widely expressed, especially in heart and skeletal muscle, skin, adipose tissue, and the ovary[24] but also in the eye (Unigene). However, the pattern of *FYCO1* expression within the eye has not previously been described. To confirm that candidate genes, including *Fyco1,* are expressed in the lens, RNA was extracted from lenses of wild-type (FVB\N strain) mice at the following stages: E8.5, E12.5, E16.5, P1, P12, P18, P21, and P35. Contamination of dissected lenses with adjacent tissue was estimated to be less than 5% by visual examination. Lens cDNA was made by RT-PCR with the SuperScriptTM III First-Strand Synthesis System (Invitrogen, Carlsbad), and direct PCR amplification of the cDNA was performed. Expression of *Fyco1* was tested by PCR analysis of lens full-length cDNA with the use of one pair of gene-specific primers, which amplify a 4317 bp product. The PCR primers (forward, 5′-ATGGCTTCTAGCAGCACTGAGA-3′; reverse, 5′-CTATGGGAAATCGCTTCCATCG-3′) are located in exons 2 and 18, respectively. PCR Products were then electrophoresed on a 1% agarose gel and visualized by ethidium bromide staining. The ubiquitously expressed *Gapdh* was used as an amplification control. No alternative splicing was detected by amplification across adjacent and multiple exons (data not shown).

In order to characterize expression of *Fyco1* in the eye lens during development, we assessed levels of *Fyco1* transcript expression in the mouse eye lens by quantitative RT-PCR of RNA and generated a 4317 bp product spanning exons 2–18 of the mouse *Fyco1* (Figure 5A). Quantitative real-time PCR was performed with SYBR Green chemistry in an ABI Prism 7900HT Sequence Detection System (Applied Biosystems, Warrington, UK). The *Fyco1* real-time PCR primers were 5′- GCACCAAGAGGCTATGACTTG-3′ and 5′- ACTACTCATGCTGGAGCTTCG-3′, producing a 117 bp PCR amplicon. The Gapdh real-time PCR primers were 5′-GGTCATCCATGACAACTTTGG-3′ and 5′-GGATG CAGGGATGATGTTCT-3′, creating a 145 bp PCR amplicon. Quantitative (q) RT-PCR was performed, and the data were analyzed according to the recommendations of the manufacturer (QIAGEN). We averaged and normalized results by dividing mean values of Fyco1 mRNA by mean values for Gapdh, the endogenous reference gene. Relative quantification analysis was performed with the comparative C_T ($2^{-\Delta\Delta CT}$) method, for which *Gapdh* was used as an endogenous control gene for PCR normalization concerning the amount of RNA added to the reverse transcription reactions. Standard deviations were calculated from three independent experiments; each real-time PCR reaction was performed four times so that data reproducibility could be assessed. Relative to levels of the internal control *Gapdh*, *FYCO1* mRNA is expressed at E8.5, in the developing lens placode. It remains relatively stable until it doubles between E12.5, at which time the lens vesicle has been formed and the primary lens fibers have elongated from the posterior wall to fill the lens vesicle, and E16.5. During this time the anterior epithelial cells divide and move to the lens equator, where they elongate and differentiate to form the secondary lens fiber cells, whose formation is associated with loss of organelles. Increasing rapidly, *FYCO1* expression then roughly doubles between

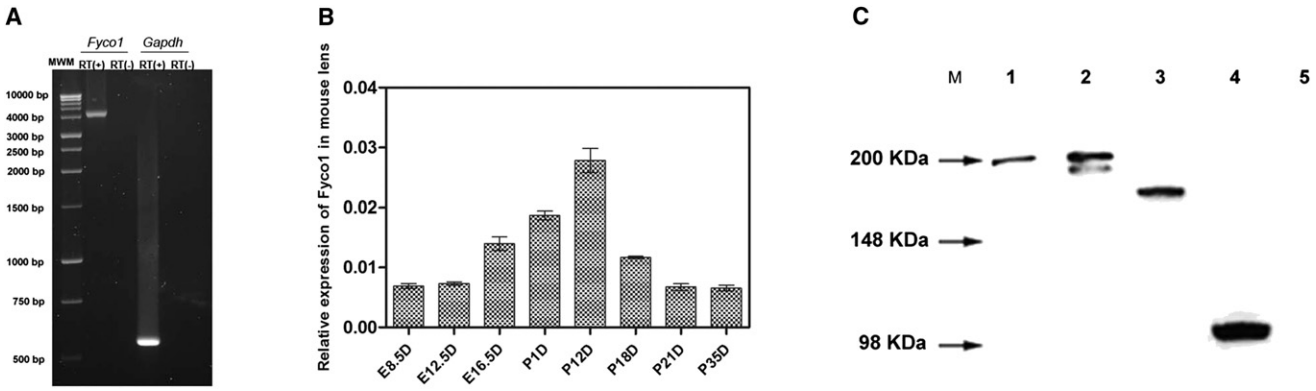

Figure 5. FYCO1 Expression in the Lens and Human Lens Cell Culture
(A) RT-PCR amplification of *Fyco1* mRNA from P3W mouse eye lens. RT (+) and RT (–) denote controls with or without reverse transcription, respectively. Lane 1, full-length *Fyco1* transcript; lane 2, negative control for *Fyco1* transcript; lane 3, *Gapdh* transcript; lane 4, negative control for *Gapdh* transcript. MWM stands for molecular-weight marker.
(B) Relative expression of *Fyco1* in mouse eye lens tissues at various ages. Expression of Fyco1 was measured in lens tissues by qRT-PCR at different time points during aging. Data represent the mean (±SD) on an arbitrary scale (*y* axis) representing expression relative to the housekeeping gene *Gapdh*.
(C) Characterization of mutant and wild-type GFP-FYCO1 by immunoblot analysis. Lane 1, transfected wild-type FYCO1-GFP lysate; lane 2, lysate transfected with mutant FYCO1-GFP (p.Leu1376Pro); lane 3, lysate transfected with mutant FYCO1-GFP (p.Leu1288TrpfsX37); lane 4, lysate transfected with mutant FYCO1-GFP (p.Gln736X); lane 5, untransfected lysate. "M" indicates molecular-weight positions of the SeeBlue2 Plus molecular-weight marker. Wild-type proteins migrate at the predicted molecular weight of 197 kDa. Missense mutant proteins migrate at the predicted molecular weight of 197 kDa. Duplication mutant proteins migrate at the predicted molecular weight of 165 kDa. Nonsense mutant proteins migrate at the predicted molecular weight of 105 kDa.

E16.5 and P12 before gradually decreasing to levels similar to those in early embryonic life (Figure 5B).

Wild-type and mutant human FYCO1-GFP fusion proteins were analyzed by immunoblotting after transient transfection of human lens epithelial cells with wild-type and mutant FYCO1-GFP constructs. The cDNA encoding the full-length wild-type FYCO1 was purchased from Origene (ORF Clones). Full-length wild-type FYCO1 cDNA was cloned into the phCMV6-AC-GFP vector, and a GFP tag was placed at the C-terminal end of the cDNA. Single point mutations were introduced into human *FYCO1* with a QuickChangeTM site directed mutagenesis kit (Stratagene, La Jolla, CA, USA). DNA sequences were verified by sequencing. The cells were harvested 48 hr after transfection. Washed cells were lysed with RIPA buffer. Immunoblot analysis was performed with 10 μg reduced proteins separated on 10% Bis-Tris gels (Invitrogen). Wild-type and L1376P missense mutant GFP-FYCO1 proteins migrate with an approximate molecular weight of 197 kDa (Figure 5C), consistent with the expected molecular mass, although the doublet below the 197 kDa band in the L1376P mutant transfected lanes might represent a degradation product. Characterization of the mutant proteins, p.Leu1288TrpfsX37 and p.Gln736X, with sizes of 165 and 105 kDa, indicated that they were truncated as predicted, (Figure 5C).

In order to localize normal and mutant human FYCO1 protein within the cell, we transfected cultured human lens epithelial cells with pCMV6-AC-FYCO1-GFP and visualized immunofluorescence with a Zeiss LSM 510 laser scanning confocal microscope. Human lens epithelial cells (FHL124[28]) were cultured in DMEM, supplemented with 10% fetal bovine serum, 2 mM glutamine, 100 units/ml penicillin, and 100 μg/ml streptomycin. They were transfected in triplicate in four-well chamber slides (Glass Chamber Slide System) with the full-length wild-type or mutant FYCO1 constructs (plasmid pCMV6-AC-FYCO1-GFP) via PolyJet (SignaGen Laboratories) according to the manufacturer's instructions. Cells were analyzed 12 hr post-transfection. They were cultured in four-well chamber slides for 12 hr incubation and then fixed in freshly prepared 4% formaldehyde for 20 min, washed twice with PBS, and incubated in blocking buffer (0.5% Tween-20, 1% bovine serum albumin, and 1% goat serum in 1× PBS) overnight in 4°C. The blocking buffer was removed, and cells were incubated with primary antibodies: mouse monoclonal anti-tubulin (Sigma-Aldrich), mouse monoclonal anti-golgin 97 (Invitrogen), and polyclonal rabbit anti-LC3antibody (Thermo Scientific Pierce Antibodies) diluted 1:2000, 1:50, and 1:100, respectively, in blocking buffer for 1 hr at room temperature. After being washed three times with PBS plus 0.05% Tween-20 (PBST), cells were incubated for 1 hr at room temperature with a second antibody, either Alexa Fluor 555 goat-anti rabbit IgG or goat-anti mouse IgG (red) diluted in buffer (0.05% Tween-20, 1% bovine serum albumin in 1× PBS). LysoTracker Red DND-99 antibody (Invitrogen, USA, 1:20000) was incubated with live transfected cells for 20 min according to the manufacturer's instructions. After being washed twice with PBS, cells were fixed in 4% paraformaldehyde. Finally, they were washed three times and covered with Gel-Mount and a coverslip. Immunofluorescence was visualized with a Zeiss LSM 700 laser scanning confocal microscope.

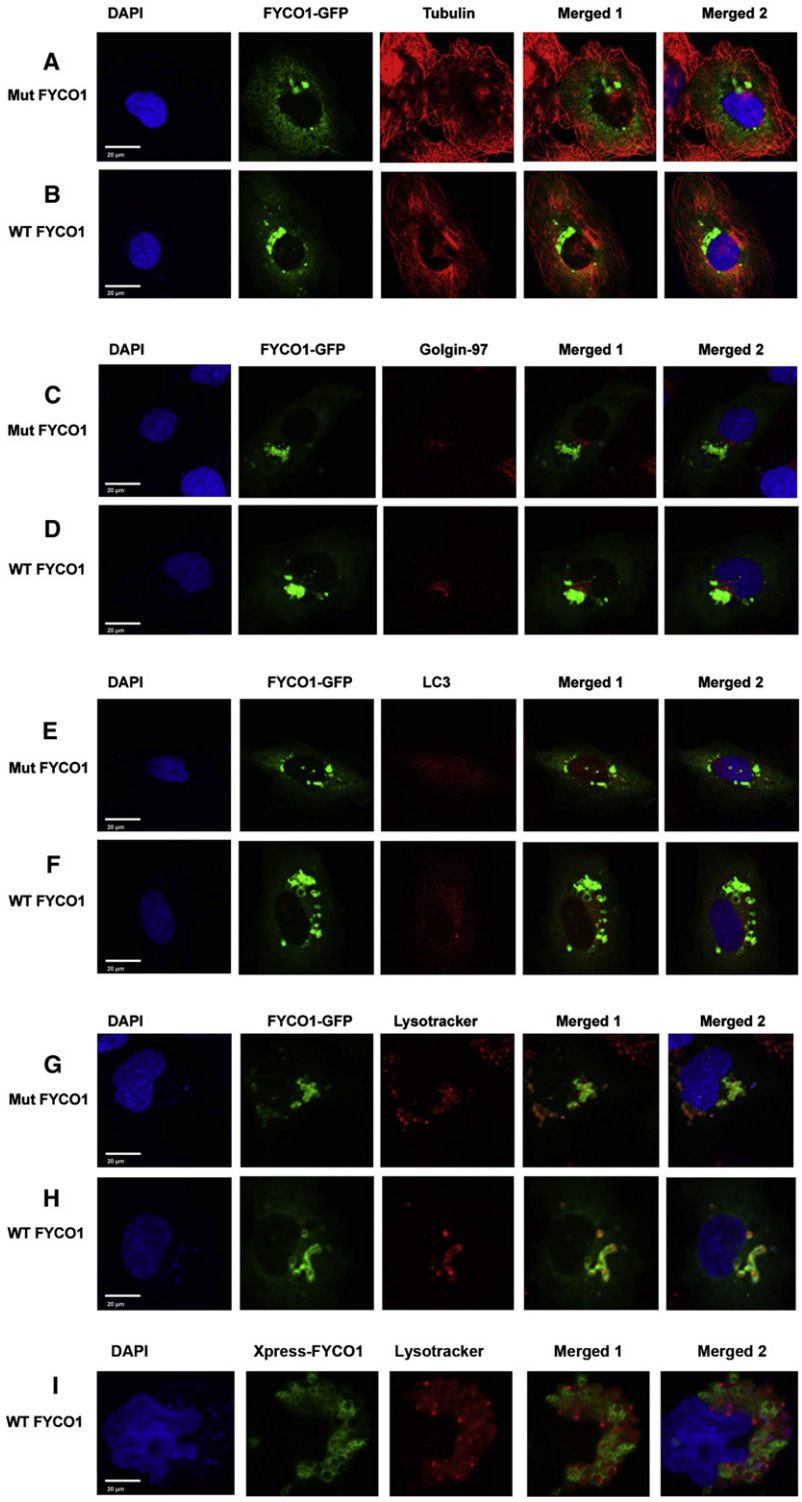

Figure 6. Immunofluorescence Images Showing Localization of Mutant and Wild-Type GFP-FYCO1 Proteins in Human Lens Epithelial Cells
Human lens epithelial cells were transfected with pCMV6-AC-FYCO1-GFP in which wild-type (B, D, F, and H) or p.Leu1376Pro mutant FYCO1 (A, C, E, and G) is fused in frame with GFP. Cells were immunostained with organelle-specific antibodies or dyes, including anti-tubulin (red, microtubules) (A and B), anti-golgin 97 (red, Golgi) (C and D), anti-LC3 (red, autophagosomes) (E and F), and LysoTracker Red DND-99 dye (red, endosomes and lysosomes) (G and H). All cells were stained with the nuclear marker DAPI (4′, 6-diamidino-2-phenylindole, blue, nucleus). R + G represents overlay of red and green channels. R + G + B depicts red, green, and blue (DAPI) channels. Scale bars represent 20 μm. Both wild-type (WT) and mutant (Mut) proteins partially colocalize adjacent to Golgi, autophagosomes, endosomes, and lysosomes of the cytoplasm of human lens epithelial cells. Wild-type Xpress-tagged FYCO1 shows similar localization (I).

Neither the wild-type nor mutant human FYCO1 colocalizes with tubulin, a microtubule marker (Figures 6A and 6B). The heaviest concentration localizes adjacent to the *trans*-Golgi compartment, as identified by golgin 97 (Figures 6C and 6D). There is faint colocalization with LC3, a marker for autophagosomes (Figures 6E and 6F) and heavy staining colocalizing with LysoTracker, a marker for endosomes and lysosomes (Figures 6G and 6H). Interestingly, although LysoTracker appears to stain the lysosomes homogeneously, FYCO1-GFP appears to be localized to the outer membranes of the lysosomes and to surround the LysoTracker stained body in a circle, consistent with the results of Pankiv et al.[29] This suggests that FYCO1 localizes to the autophagosomes, endosomes, and lysosomes and also suggests that the p.L1376P mutation does not affect localization of FYCO1. To ensure that localization of FYCO1-GFP was not affected by the proximity of the GFP tag to the GOLD domain, we cloned wild-type FYCO1 into into pcDNA4/HisMax C between Kpn1 and Not1, which has an Xpress tag before the FYCO1 sequence, expressed it in human lens epithelial cells, and detected it as above. Localization of the Xpress-tagged FYCO1 was similar to that of the GFP-tagged protein, although there might be a more even distribution of lysosomal staining (Figure 6I).

The CATC2 locus was first mapped to chromosome 3 in 2001 by Pras et al.,[19] but the disease-associated variant had not been identified. In this study, arCC in twelve unrelated Pakistani families has been mapped to a 3.5 cM (12 Mb) chromosomal region, 3p21, flanked by *D3S3685* and *D3S1289*, which overlaps with the CATC2 locus described by Pras et al.[19] arCC in these families and in family 1 from Pras et al.[19] has been associated with mutations in *FYCO1*, the gene encoding a protein important for transport of autophagocytic vesicles. In total, nine different *FYCO1* mutations were identified in 13 (12 Pakistani and one Arab Israeli) arCC families

including 44 affected individuals, in all of which the disease segregates with the mutant allele. As part of an ongoing collaboration to study arCC in Pakistan, we have studied 125 familial cases of arCC, and *FYCO1* is responsible for approximately 10% to the total genetic load of congenital cataracts in our study, and possibly in the Pakistani population as well, which would mean that *FYCO1* mutations are among the most common causes of inherited congenital cataracts in the Pakistani population as a whole. In addition, identification of a *FYCO1* mutation in an Arab Israeli family indicates that disruption of this gene is a cause of arCC in additional populations as well. This will be further clarified as *FYCO1* is screened in other populations.

Autophagy is associated with a variety of disease processes, including tumorigenesis, neurodegenerative diseases, cardiomyopathy, Crohn disease, fatty liver, type II diabetes, defense against intracellular pathogens, antigen-presentation, and longevity.[30–33] Among the proteins and multimolecular complexes that contribute to autophagosome formation are PI(3)-binding proteins, PI3-phosphatases, Rabs, the Atg1/ULK1 protein-kinase complex, the Vps34-Atg6/beclin1 class III PI3-kinase complex, and the Atg12 and Atg8/LC3 conjugation systems. Soon after an autophagosome forms, its outer membrane fuses with lysosomes to form autolysosomes, a process requiring Rab7.[34,35] FYCO1 was independently identified as a Rab7 effector and a PI(3)P-binding protein and was found to associate with the exterior of autophagosomes via its FYVE domain. Pankiv et al. have recently reported that depletion of FYCO1 leads to perinuclear accumulation of residual autophagosomes, and proposed a role for FYCO1 in tethering autophagosomes to plus-end-directed microtubule motor proteins to explain this phenotype. FYCO1 also interacts preferentially with GTP-bound Rab7, the GTPase implicated in autophagosome-lysosomal fusion, and Rab7 recruits FYCO1 to autophagosomes.[29,36] This suggests that FYCO1 mediates microtubule plus-end-directed movement of autophagosomes. In transfected human lens epithelial cells, FYCO1 proteins localize to lysosomes and autophagosomes, particularly near the Golgi complex in the perinuclear area (Figure 6). Behrends et al. found that FYCO1 associates with two microtubule motor proteins, kinesin (KIF) 5B and KIF23.[37] Interestingly, depletion of KIF5B leads to perinuclear accumulation of autophagosomes, allowing Behrends et al. to propose that KIF5B links FYCO1-positive autophagosomes to microtubules to maintain cortical localization.[38] Behrends et al. also showed that C7orf28A associates with FYCO1. C7orf28A depletion led to an increase in autophagosome number without blocking autophagosomal flux.[37] Thus, FYCO1 seems to function as a platform for assembly of vesicle fusion and trafficking factors.

The high frequency of frameshift, splice, and nonsense mutations and the recessive inheritance pattern seen in the families suggest that arCC in these families results from loss of FYCO1 function. Loss of functional FYCO1 could lead to arCC through a variety of mechanisms. Autophagy is important for degradation of aggregated misfolded proteins, and accumulation of protein aggregates is a classic mechanism for light scattering and loss of lens transparency. It is also possible that loss of FYCO1 inhibits transport of autophagosomes from the perinuclear area to the periphery and leads to an accumulation of large numbers of vesicles and hence loss of transparency. Perhaps most intriguing is the possibility that loss of FYCO1 activity inhibits the organelle degradation that is an integral part of differentiation of epithelial cells into lens fiber cells. This would help to explain the specific effect of the absence of functional FYCO1 on the lens even though it is widely expressed in the body. In any event, identification of FYCO1 as a cause of congenital cataracts suggests that autophagy is critically important for lens transparency.

In summary, we report localization of an arCC locus in 12 families of Pakistani origin and one Arab Israeli family to a 3.5 cM (12 Mb) chromosomal region, 3p21-p22, and identification of pathogenic mutations in *FYCO1*, which has been shown to affect intracellular transport of autophagocytic vesicles. This study provides a new cellular and molecular entry point for understanding lens transparency and human cataracts and because of the frequency of FYCO1 mutations in the Pakistani population might be useful in genetic diagnosis and eventually better cataract treatment or prevention.

Supplemental Data

Supplemental Data include one figure and three tables and can be found with this article online at http://www.cell.com/AJHG/.

Acknowledgments

The authors are thankful to all the family members for their participation in this study and to James Friedman for advice and assistance with the fluorescent localization studies. This study was supported in part by the Higher Education Commission and Ministry of Science and Technology, Islamabad, Pakistan. This work was also supported by the NIH grant ey13022, National Academy of Sciences, and the U.S. Department of State, Washington, DC, USA (Note: All findings and conclusions are those of the authors and do not necessarily reflect the views of the National Academy of Sciences or the U.S. Department of State).

Received: March 18, 2011
Revised: April 29, 2011
Accepted: May 9, 2011
Published online: June 2, 2011

Web Resources

The URLs for data presented herein are as follows:

GeneCards http://www.genecards.org/
Marshfield Clinic Research Foundation, http://www.marshfieldclinic.org/research/pages/index.aspx
Multiple Sequence Alignment Program, http://www.ebi.ac.uk/Tools/clustalw2/index.html

NCBI http://www.ncbi.nlm.nih.gov/Database/index.html
NCBI UniGene http://www.ncbi.nlm.nih.gov/unigene/
Online Mendelian Inheritance in Man (OMIM), http://www.omim.org
PolyPhen program, http://genetics.bwh.harvard.edu/pph/
Primer3 program, http://primer3.sourceforge.net/
Splice Site Score Calculation, http://rulai.cshl.edu/new_alt_exon_db2/HTML/score.html
UCSC Genome Bioinformatics, http://genome.ucsc.edu

Reference

1. Robinson, G.C., Jan, J.E., and Kinnis, C. (1987). Congenital ocular blindness in children, 1945 to 1984. Am. J. Dis. Child. *141*, 1321–1324.
2. Hejtmancik, J.F. (2008). Congenital cataracts and their molecular genetics. Semin. Cell Dev. Biol. *19*, 134–149.
3. Lambert, S.R., and Drack, A.V. (1996). Infantile cataracts. Surv. Ophthalmol. *40*, 427–458.
4. Foster, A. (1999). Cataract—A global perspective: output, outcome and outlay. Eye (Lond.) *13* (Pt 3b), 449–453.
5. François, J. (1982). Genetics of cataract. Ophthalmologica *184*, 61–71.
6. Haargaard, B., Wohlfahrt, J., Fledelius, H.C., Rosenberg, T., and Melbye, M. (2004). A nationwide Danish study of 1027 cases of congenital/infantile cataracts: etiological and clinical classifications. Ophthalmology *111*, 2292–2298.
7. Merin, S. (1991). Inherited Cataracts. In Inherited Eye Diseases, S. Merin, ed. (New York: Marcel Dekker,Inc.), pp. 86–120.
8. Shiels, A., Bennett, T.M., and Hejtmancik, J.F. (2010). CatMap: Putting cataract on the map. Mol. Vis. *16*, 2007–2015.
9. Cohen, D., Bar-Yosef, U., Levy, J., Gradstein, L., Belfair, N., Ofir, R., Joshua, S., Lifshitz, T., Carmi, R., and Birk, O.S. (2007). Homozygous CRYBB1 deletion mutation underlies autosomal recessive congenital cataract. Invest. Ophthalmol. Vis. Sci. *48*, 2208–2213.
10. Kaul, H., Riazuddin, S.A., Shahid, M., Kousar, S., Butt, N.H., Zafar, A.U., Khan, S.N., Husnain, T., Akram, J., Hejtmancik, J.F., and Riazuddin, S. (2010). Autosomal recessive congenital cataract linked to EPHA2 in a consanguineous Pakistani family. Mol. Vis. *16*, 511–517.
11. Ponnam, S.P., Ramesha, K., Tejwani, S., Ramamurthy, B., and Kannabiran, C. (2007). Mutation of the gap junction protein alpha 8 (GJA8) gene causes autosomal recessive cataract. J. Med. Genet. *44*, e85.
12. Ponnam, S.P., Ramesha, K., Tejwani, S., Matalia, J., and Kannabiran, C. (2008). A missense mutation in LIM2 causes autosomal recessive congenital cataract. Mol. Vis. *14*, 1204–1208.
13. Pras, E., Frydman, M., Levy-Nissenbaum, E., Bakhan, T., Raz, J., Assia, E.I., Goldman, B., and Pras, E. (2000). A nonsense mutation (W9X) in CRYAA causes autosomal recessive cataract in an inbred Jewish Persian family. Invest. Ophthalmol. Vis. Sci. *41*, 3511–3515.
14. Pras, E., Levy-Nissenbaum, E., Bakhan, T., Lahat, H., Assia, E., Geffen-Carmi, N., Frydman, M., Goldman, B., and Pras, E. (2002). A missense mutation in the LIM2 gene is associated with autosomal recessive presenile cataract in an inbred Iraqi Jewish family. Am. J. Hum. Genet. *70*, 1363–1367.
15. Pras, E., Raz, J., Yahalom, V., Frydman, M., Garzozi, H.J., Pras, E., and Hejtmancik, J.F. (2004). A nonsense mutation in the glucosaminyl (N-acetyl) transferase 2 gene (GCNT2): Association with autosomal recessive congenital cataracts. Invest. Ophthalmol. Vis. Sci. *45*, 1940–1945.
16. Ramachandran, R.D., Perumalsamy, V., and Hejtmancik, J.F. (2007). Autosomal recessive juvenile onset cataract associated with mutation in BFSP1. Hum. Genet. *121*, 475–482.
17. Riazuddin, S.A., Yasmeen, A., Yao, W., Sergeev, Y.V., Zhang, Q., Zulfiqar, F., Riaz, A., Riazuddin, S., and Hejtmancik, J.F. (2005). Mutations in betaB3-crystallin associated with autosomal recessive cataract in two Pakistani families. Invest. Ophthalmol. Vis. Sci. *46*, 2100–2106.
18. Smaoui, N., Beltaief, O., BenHamed, S., M'Rad, R., Maazoul, F., Ouertani, A., Chaabouni, H., and Hejtmancik, J.F. (2004). A homozygous splice mutation in the HSF4 gene is associated with an autosomal recessive congenital cataract. Invest. Ophthalmol. Vis. Sci. *45*, 2716–2721.
19. Pras, E., Pras, E., Bakhan, T., Levy-Nissenbaum, E., Lahat, H., Assia, E.I., Garzozi, H.J., Kastner, D.L., Goldman, B., and Frydman, M. (2001). A gene causing autosomal recessive cataract maps to the short arm of chromosome 3. Isr. Med. Assoc. J. *3*, 559–562.
20. Grimberg, J., Nawoschik, S., Belluscio, L., McKee, R., Turck, A., and Eisenberg, A. (1989). A simple and efficient non-organic procedure for the isolation of genomic DNA from blood. Nucleic Acids Res. *17*, 8390.
21. Cottingham, R.W., Jr., Idury, R.M., and Schäffer, A.A. (1993). Faster sequential genetic linkage computations. Am. J. Hum. Genet. *53*, 252–263.
22. Lathrop, G.M., and Lalouel, J.M. (1984). Easy calculations of lod scores and genetic risks on small computers. Am. J. Hum. Genet. *36*, 460–465.
23. Kiss, H., Darai, E., Kiss, C., Kost-Alimova, M., Klein, G., Dumanski, J.P., and Imreh, S. (2002). Comparative human/murine sequence analysis of the common eliminated region 1 from human 3p21.3. Mamm. Genome *13*, 646–655.
24. Kiss, H., Yang, Y., Kiss, C., Andersson, K., Klein, G., Imreh, S., and Dumanski, J.P. (2002). The transcriptional map of the common eliminated region 1 (C3CER1) in 3p21.3. Eur. J. Hum. Genet. *10*, 52–61.
25. Marchler-Bauer, A., Anderson, J.B., Chitsaz, F., Derbyshire, M.K., DeWeese-Scott, C., Fong, J.H., Geer, L.Y., Geer, R.C., Gonzales, N.R., Gwadz, M., et al. (2009). CDD: specific functional annotation with the Conserved Domain Database. Nucleic Acids Res. *37* (Database issue), D205–D210.
26. Lupas, A., Van, D.M., and Stock, J. (1991). Predicting coiled coils from protein sequences. Science *252*, 1162–1164.
27. Rose, A., Schraegle, S.J., Stahlberg, E.A., and Meier, I. (2005). Coiled-coil protein composition of 22 proteomes—Differences and common themes in subcellular infrastructure and traffic control. BMC Evol. Biol. *5*, 66.
28. Wormstone, I.M., Tamiya, S., Marcantonio, J.M., and Reddan, J.R. (2000). Hepatocyte growth factor function and c-Met expression in human lens epithelial cells. Invest. Ophthalmol. Vis. Sci. *41*, 4216–4222.
29. Pankiv, S., Alemu, E.A., Brech, A., Bruun, J.A., Lamark, T., Overvatn, A., Bjørkøy, G., and Johansen, T. (2010). FYCO1 is a Rab7 effector that binds to LC3 and PI3P to mediate microtubule plus end-directed vesicle transport. J. Cell Biol. *188*, 253–269.
30. Eskelinen, E.L., and Saftig, P. (2009). Autophagy: A lysosomal degradation pathway with a central role in health and disease. Biochim. Biophys. Acta *1793*, 664–673.
31. Levine, B., and Kroemer, G. (2008). Autophagy in the pathogenesis of disease. Cell *132*, 27–42.

32. Mizushima, N., Levine, B., Cuervo, A.M., and Klionsky, D.J. (2008). Autophagy fights disease through cellular self-digestion. Nature *451*, 1069–1075.
33. Münz, C. (2009). Enhancing immunity through autophagy. Annu. Rev. Immunol. *27*, 423–449.
34. Gutierrez, M.G., Munafó, D.B., Berón, W., and Colombo, M.I. (2004). Rab7 is required for the normal progression of the autophagic pathway in mammalian cells. J. Cell Sci. *117*, 2687–2697.
35. Jäger, S., Bucci, C., Tanida, I., Ueno, T., Kominami, E., Saftig, P., and Eskelinen, E.L. (2004). Role for Rab7 in maturation of late autophagic vacuoles. J. Cell Sci. *117*, 4837–4848.
36. Pankiv, S., and Johansen, T. (2010). FYCO1: Linking autophagosomes to microtubule plus end-directing molecular motors. Autophagy *6*, 550–552.
37. Behrends, C., Sowa, M.E., Gygi, S.P., and Harper, J.W. (2010). Network organization of the human autophagy system. Nature *466*, 68–76.
38. Cardoso, C.M., Groth-Pedersen, L., Høyer-Hansen, M., Kirkegaard, T., Corcelle, E., Andersen, J.S., Jäättelä, M., and Nylandsted, J. (2009). Depletion of kinesin 5B affects lysosomal distribution and stability and induces peri-nuclear accumulation of autophagosomes in cancer cells. PLoS ONE *4*, e4424.